Advances in Applied Mathematics and Mechanics
Adv. Appl. Math. Mech., Vol. **x**, No. 1, pp. 1-26

DOI: 10.4208/aamm.OA-2022-0144
xxx 2025

High Order Well-Balanced Finite Difference AWENO Scheme for Ripa and Pollutant Transport Systems

Yue Liu[1], Zhen Gao[1], Peng Li[2] and Yaguang Gu[3,*]

[1] *School of Mathematical Sciences, Ocean University of China, Qingdao, Shandong 266100, China*
[2] *Department of Engineering Mechanics, Shijiazhuang Tiedao University, Shijiazhuang, Hebei 050043, China*
[3] *School of Mathematics, South China University of Technology, Guangzhou, Guangdong 510641, China*

Received 28 May 2022; Accepted (in revised version) 30 October 2022

Abstract. The Ripa model consists of the shallow water equations and terms which take the horizontal temperature fluctuations into account. The pollutant transport model describes the transport and diffusion of pollutants in shallow water flows. Both models admit hydrostatic solutions in which the gradient of the flux term is exactly balanced by the source term on the right-hand side. In this paper, we write both models in a unified form and propose a well-balanced fifth-order finite difference alternative weighted essentially non-oscillatory (AWENO) scheme, which allows using arbitrary monotone, Lipschitz continuous and consistent numerical flux. For illustration purposes, the Lax-Friedrichs flux is employed. In order to design a well-balanced AWENO scheme, reformulation of the source term and linearization of the WENO interpolation operator are made. The well-balancedness of the proposed method will be analysed theoretically in this paper. Numerical examples verify the well-balanced property, high-order accuracy and effectiveness of our approach.

AMS subject classifications: 35L65, 65M06, 76M20

Key words: AWENO scheme, well-balanced, Ripa model, pollutant transport model.

1 Introduction

The shallow water equations (SWEs) are attractive among researchers due to their wide range of applications in describing the flood waves, dam breaks and tidal flows in coastal regions. A tremendous amount of numerical approaches for the shallow water equations

*Corresponding author.
Emails: liuyue6091@stu.ouc.edu.cn (Y. Liu), zhengao@ouc.edu.cn (Z. Gao), pengli@stdu.edu.cn (P. Li), guyaguang@scut.edu.cn (Y. Gu)

were developed in the recent literature, and readers are referred to [1,9,11–14,26,28,36] and references therein.

In this paper, we study two models related to the shallow water equations, i.e., the Ripa model and the pollutant transport model. The Ripa model, which was introduced in [17,31,32] to model ocean currents when temperature fluctuations play an important role, consists of the SWEs and terms which take the horizontal temperature fluctuations into account. The governing equations of the systems are derived by integrating vertically the velocity fields, density, and horizontal pressure gradient in each layer of the multi-layer model. Since the motion and behavior of the currents are influenced by forces such as temperature acting on the water, a horizontal temperature gradient is introduced to represent the variation in fluid density. This demonstrates the importance of the study on the Ripa model for understanding real-world phenomena. The pollutant transport model, which was studied in [2,10], comprises SWEs and terms which concern transport of a passive pollutant in the flow modeled by the Saint-Venant system. Due to the fact that the transport of pollutants in rivers, reservoirs, oceans and some coastal areas may have harmful effects on the environment, it is necessary to predict the transport of pollutants, find their location and concentration, and provide accurate and reliable estimates, which would significantly help to improve the environment.

For simplicity, the Ripa model and the pollutant transport model can be written into a unified form,

$$\frac{\partial \mathbf{Q}}{\partial t}+\nabla\cdot\mathbf{F}(\mathbf{Q})=\mathbf{S}(\mathbf{Q},b), \tag{1.1}$$

where $\mathbf{Q}$, $\mathbf{F}(\mathbf{Q})$ and $\mathbf{S}(\mathbf{Q},b)$ are vectors of conservative variables, flux and source, respectively, with

$$\mathbf{Q}=\begin{pmatrix} h \\ h\mathbf{u} \\ h\xi \end{pmatrix}, \quad \mathbf{F}(\mathbf{Q})=\begin{pmatrix} h\mathbf{u} \\ h\mathbf{u}\otimes\mathbf{u}+\dfrac{1}{2}gh^2\phi(\xi)\mathbf{I}_d \\ h\xi\mathbf{u} \end{pmatrix}, \quad \mathbf{S}(\mathbf{Q},b)=\begin{pmatrix} 0 \\ -gh\phi(\xi)\nabla b \\ 0 \end{pmatrix}. \tag{1.2}$$

with

$$\xi=\begin{cases}\theta, & \text{Ripa model,}\\ T, & \text{Pollutant transport model,}\end{cases} \qquad \phi(\xi)=\begin{cases}\theta, & \text{Ripa model,}\\ 1, & \text{Pollutant transport model,}\end{cases}$$

where d is the dimension of the space, h denotes the water height, $\mathbf{u}$ is the water velocity, θ is the temperature, T is the pollutant concentration, g is the gravitational constant and $b=b(x)$ denotes the bottom topography. Here we consider the dimensionless model. In addition, $h+b$ stands for the water surface. A notable feature of the system (1.1) is that both models admit the following steady state solutions,

$$h+b=\text{constant}, \quad \mathbf{u}=0, \quad \xi=\text{constant}. \tag{1.3}$$

This is usually called *C-property*, where "C" stands for "constant". At the discrete level, a scheme which preserves the C-property is referred to as a *well-balanced* scheme. The

advantages of using a well-balanced scheme can be found in [41]. The most important advantage of a well-balanced scheme is that it can accurately resolve small perturbations of a steady state solution on relatively coarse meshes.

The difficulty is that the solution of both systems may contain non-linear shock waves, rarefaction waves and linear discontinuities, so that the solution itself is usually not smooth. Even worse, if the bottom is non-flat, their interactions may lead to very complex wave structures and non-trivial equilibria, which are numerically difficult to maintain. Therefore, designing an reliable numerical method for this model is a challenging task but critical. For the Ripa model, Chertock et al. built a well-balanced and positivity-preserving central upwind scheme in [15], in which an interface tracking method is coupled. Desveaux et al. proposed in [18] a relaxation technique and exhibited an approximate Riemann solver to design a well-balanced scheme for Ripa model. In [35], a new well-balanced central finite volume scheme was introduced both in one and two dimensions. In [21], the authors designed a high order well-balanced finite difference weighted essentially non-oscillatory (WENO) scheme for the Ripa model where high-order accuracy was achieved by using the traditional WENO reconstruction technique. For the pollutant transport model, Kurganov and Levy proposed in [23] a central-upwind scheme for approximating solutions of the Saint-Venant system. In [24], a well-balanced finite difference WENO scheme is presented for modelling transport and diffusion of pollutant in shallow water flows. Qian et al. introduced in [29] a central WENO scheme for the sediment transport model in shallow water. In [16], a finite-volume-particle method was proposed where they used finite volume methods for the shallow water equations and particle method for the transport equation of pollutant. Xu and Shu applied the anti-diffusive high order WENO scheme to the pollutant transport model in [42].

Our aim of this paper is to design a well-balanced high order finite difference alternative weighted essentially non-oscillatory (AWENO) scheme [22,39] for the Ripa model and the pollutant transport model. Compared with the classical WENO schemes [4–8], the AWENO scheme requires polynomial interpolation procedure on the conservative variables rather than flux reconstruction procedure in the classical finite difference WENO scheme. The advantage of the AWENO scheme is that arbitrary monotone, Lipschitz continuous and consistent numerical flux can be applied to the framework [27], and it provides superior free-stream and vortex preservation on the generalized curvilinear meshes easily, whereas only the smooth flux splitting can be used to reconstruct the flux functions in the classical finite difference WENO formulation. Besides, the AWENO scheme has higher resolution, less dissipation and dispersion errors than classical WENO schemes. Moreover, the AWENO scheme has potential in designing well-balanced and equilibrium-preserving methods for a variety of models in compressible fluid dynamics, e.g., [19, 20, 38]. However, direct use of the AWENO scheme does not lead to a well-balanced discretization. As a result, the C-property is not satisfied. To remedy this drawback, we mimic [40] to reformulate the source term. The idea is to rewrite h into $(h+b)-b$ since the water surface $h+b$ and the bottom topography b do not change with time when solutions are at the steady state (1.3). Besides, we linearize the WENO interpolation op-

erator in the sense that the non-linear weights for the bottom topography b are the same as those for the water depth h. As a result, the water surface would always be a constant when the flow is hydrostatic. We then prove that the proposed method is well-balanced. Finally, a variety of numerical examples verify our theory and indicate that our approach has potentials in capturing basic physical structures, i.e., rarefaction and shock waves, for more general problems, e.g., shock-tube problem, small perturbations imposed on steady-state solutions, dam break simulations, etc.

The rest of this paper is organized as follows. In Section 2, we revisit the traditional fifth-order finite difference AWENO scheme and introduce how to apply it to the model (1.1). Then well-balanced modifications of the source term in (1.1) and the AWENO scheme are introduced in Section 3, where a unified framework is discussed for both the Ripa and pollutant transport models. A variety of numerical examples illustrate the high-order of accuracy and effectiveness of our approach in Section 4 and Section 5 for the Ripa and pollutant transport models, respectively. Finally, conclusions will be given in Section 6.

2 Traditional fifth-order finite difference AWENO scheme

Let $\Omega=[a,b]$ be the computational domain, and let $\Omega=\cup I_i$ be a uniform partition of the computational domain Ω, with $I_i:=[x_{i-\frac{1}{2}},x_{i+\frac{1}{2}}]$, $i=1,2,\cdots,N_x$. Here $x_{i+\frac{1}{2}}$ are the cell interfaces, with finite difference nodes being defined by $x_i=x_{i-\frac{1}{2}}+\frac{\Delta x}{2}$, where $\Delta x=(b-a)/N_x$ is the length of the cell I_i.

In the following subsections, the fifth-order finite difference AWENO scheme is introduced for the model (1.1).

2.1 Discretization of the term $\partial\Psi/\partial x$ ($\Psi\in\{\mathbf{F},b\}$)

The traditional conservative discretization of the term $\partial\Psi/\partial x$, where $\Psi\in\{\mathbf{F},b\}$, reads

$$\frac{\partial\Psi}{\partial x}(x_i)=\frac{1}{\Delta x}\left(\Psi_{i+\frac{1}{2}}-\Psi_{i-\frac{1}{2}}\right), \tag{2.1}$$

with $\Psi_{i+\frac{1}{2}}$ being defined at cell interfaces. According to [33], the following formula provides a sixth-order approximation of $\Psi_{i\pm\frac{1}{2}}$,

$$\Psi_{i\pm\frac{1}{2}}\approx\widehat{\Psi}_{i\pm\frac{1}{2}}=\Psi^{(0)}_{i\pm\frac{1}{2}}\underbrace{-\frac{1}{24}\Delta x^2\Psi^{(2)}_{i\pm\frac{1}{2}}+\frac{7}{5760}\Delta x^4\Psi^{(4)}_{i\pm\frac{1}{2}}}_{:=\mathcal{D}_{i\pm\frac{1}{2}}[\Psi]}, \tag{2.2}$$

where the superscripts represent the orders of spatial derivatives, and the linear operator $\mathcal{D}$ is used to denote high-order terms. Since $\Psi^{(0)}_{i\pm\frac{1}{2}}$, $\Psi^{(2)}_{i\pm\frac{1}{2}}$ and $\Psi^{(4)}_{i\pm\frac{1}{2}}$ are unknown, they

need to be approximated so that the numerical discretization is an overall fifth-order approximation of $\partial\Psi/\partial x|_{x_i}$. To this end, we adopt in this paper the fifth-order AWENO discretization [22,39], i.e., at each cell interface $x=x_{i+\frac{1}{2}}$ one has

$$\Psi^{(0)}_{i+\frac{1}{2}} \approx \begin{cases} \Psi^{\mathrm{RP}}_{i+\frac{1}{2}}\left(\mathbf{Q}^-_{i+\frac{1}{2}},\mathbf{Q}^+_{i+\frac{1}{2}}\right), & \text{if } \Psi=\mathbf{F}, \\ \dfrac{1}{2}\left(\Psi^-_{i+\frac{1}{2}}+\Psi^+_{i+\frac{1}{2}}\right), & \text{if } \Psi=b, \end{cases} \tag{2.3a}$$

$$\Delta x^2\Psi^{(2)}_{i+\frac{1}{2}} \approx \frac{1}{48}(-5\Psi_{i-2}+39\Psi_{i-1}-34\Psi_i-34\Psi_{i+1}+39\Psi_{i+2}-5\Psi_{i+3}), \tag{2.3b}$$

$$\Delta x^4\Psi^{(4)}_{i+\frac{1}{2}} \approx \frac{1}{2}(\Psi_{i-2}-3\Psi_{i-1}+2\Psi_i+2\Psi_{i+1}-3\Psi_{i+2}+\Psi_{i+3}), \tag{2.3c}$$

where $\Psi^{(2)}_{i+\frac{1}{2}}$ and $\Psi^{(4)}_{i+\frac{1}{2}}$ are the second and the fourth derivatives of Ψ at $x=x_{i+\frac{1}{2}}$, respectively, $\mathbf{Q}^-_{i+\frac{1}{2}}$ and $\mathbf{Q}^+_{i+\frac{1}{2}}$ are fifth-order approximations of $\mathbf{Q}_{i+\frac{1}{2}}$ produced by WENO interpolation which will be introduced in the next section, $\mathbf{F}^{\mathrm{RP}}_{i+\frac{1}{2}}(\mathbf{Q}^-_{i+\frac{1}{2}},\mathbf{Q}^+_{i+\frac{1}{2}})$ is an approximate solution to the Riemann problem associated with the left and right initial states $\mathbf{Q}^-_{i+\frac{1}{2}}$ and $\mathbf{Q}^+_{i+\frac{1}{2}}$, respectively. In this paper, the Lax-Friedrichs numerical flux is employed, i.e.,

$$\mathbf{F}^{\mathrm{RP}}_{i+\frac{1}{2}}\left(\mathbf{Q}^-_{i+\frac{1}{2}},\mathbf{Q}^+_{i+\frac{1}{2}}\right)=\frac{1}{2}\left(\mathbf{F}(\mathbf{Q}^-_{i+\frac{1}{2}})+\mathbf{F}(\mathbf{Q}^+_{i+\frac{1}{2}})\right)-\frac{\alpha}{2}\left(\mathbf{Q}^+_{i+\frac{1}{2}}-\mathbf{Q}^-_{i+\frac{1}{2}}\right), \tag{2.4}$$

where $\alpha=\max_i\{|u^n_i|+c^n_i\}$ and $c=\sqrt{gh\phi(\xi)}$ is the speed of sound.

2.2 WENO interpolation

In this section, the fifth order WENO interpolation procedure is briefly reviewed. Details can be found in [39]. We only show computation of $q^-_{i+\frac{1}{2}}$, where q is a variable to be interpolated. Computation of $q^+_{i+\frac{1}{2}}$ can be done in a mirror-symmetric way.

The WENO interpolation is based on the large stencil $S^5=\{q_{i-2},q_{i-1},q_i,q_{i+1},q_{i+2},q_{i+3}\}$ with its sub-stencils $S_0=\{q_{i-2},q_{i-1},q_i\}$, $S_1=\{q_{i-1},q_i,q_{i+1}\}$ and $S_2=\{q_i,q_{i+1},q_{i+2}\}$, see

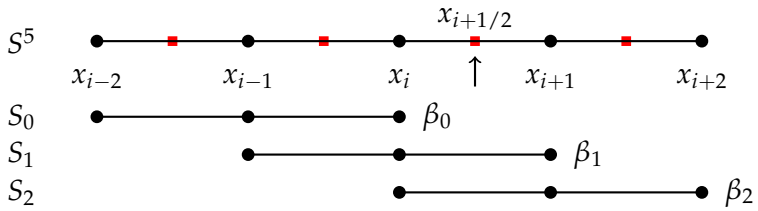

Figure 1: The grid points, stencil S^5 and its sub-stencils S_0, S_1, S_2, used in the fifth order WENO interpolation procedure.

Fig. 1. Then a second-degree polynomial, denoted by $W^-_{i+\frac{1}{2}}[q]$, is constructed on S^5 by a convex combination of three second-degree Lagrange interpolation polynomials $q^{(k)}(x)$ constructed respectively on the stencils S_0, S_1 and S_2, such that the function value of this polynomial is a fifth-order approximation of $q(x_{i+\frac{1}{2}})$, i.e.,

$$q(x_{i+\frac{1}{2}}) \approx q^-_{i+\frac{1}{2}} = W^-_{i+\frac{1}{2}}[q] = \sum_{k=0}^{2} d_k q^{(k)}(x_{i+\frac{1}{2}}), \tag{2.5}$$

where d_k are optimal (linear) weights with $\{d_0 = 1/16,\ d_1 = 5/8,\ d_2 = 5/16\}$ and explicit form of $q^{(k)}(x_{i+\frac{1}{2}})$ are

$$q^{(0)}(x_{i+\frac{1}{2}}) = \frac{3}{8}q_{i-2} - \frac{5}{4}q_{i-1} + \frac{15}{8}q_i, \tag{2.6a}$$

$$q^{(1)}(x_{i+\frac{1}{2}}) = -\frac{1}{8}q_{i-1} + \frac{3}{4}q_i + \frac{3}{8}q_{i+1}, \tag{2.6b}$$

$$q^{(2)}(x_{i+\frac{1}{2}}) = \frac{3}{8}q_i + \frac{3}{4}q_{i+1} - \frac{1}{8}q_{i+2}. \tag{2.6c}$$

To avoid numerical oscillations near discontinuities, the optimal weights are replaced by the non-linear weights ω_k. Here we adopt the one designed in [4, 39] (i.e., Z-type non-linear weights):

$$\omega_k = \frac{\alpha_k}{\sum_{s=0}^{2}\alpha_s}, \qquad \alpha_k = d_k\left(1 + \left(\frac{\tau_5}{\beta_k + \epsilon}\right)^2\right), \tag{2.7}$$

where ϵ is a sensitivity parameter being used to avoid a division by zero, $\tau_5 = |\beta_0 - \beta_2|$ is the global (on S^5) optimal-order smoothness indicator with local (on S_k) smoothness indicators β_k being explicitly computed by

$$\beta_0 = \frac{13}{12}(q_{i-2} - 2q_{i-1} + q_i)^2 + \frac{1}{4}(q_{i-2} - 4q_{i-1} + 3q_i)^2, \tag{2.8a}$$

$$\beta_1 = \frac{13}{12}(q_{i-1} - 2q_i + q_{i+1})^2 + \frac{1}{4}(q_{i-1} - q_{i+1})^2, \tag{2.8b}$$

$$\beta_2 = \frac{13}{12}(q_i - 2q_{i+1} + q_{i+2})^2 + \frac{1}{4}(3q_i - 4q_{i+1} + q_{i+2})^2. \tag{2.8c}$$

It is suggested in [3, 30] that the WENO operator should used in characteristic space to reduce spurious oscillations. For the system (1.1), the eigenvalues of the Jacobian matrix $\partial \mathbf{F}(\mathbf{Q})/\partial Q$ are

$$\lambda_1 = u, \qquad \lambda_2 = u - c, \qquad \lambda_3 = u + c,$$

where $c = \sqrt{gh\phi(\xi)}$ is the speed of sound. The left and right eigenvectors $\mathbf{l}_k$ and $\mathbf{r}_k$ corre-

sponding to λ_k form the following left and right eigen-matrices, respectively,

$$\mathbf{L}=\begin{pmatrix}\mathbf{l}_1\\ \mathbf{l}_2\\ \mathbf{l}_3\end{pmatrix}=\begin{pmatrix}-\frac{\xi\eta(\xi)}{2\phi(\xi)} & 0 & \frac{\eta(\xi)}{2\phi(\xi)}\\ \frac{\xi(2\phi(\xi)u+\eta(\xi)c)}{4\phi(\xi)c} & \frac{-\xi}{2c} & \frac{\xi\phi'(\xi)}{4\phi(\xi)}\\ \frac{-\xi(2\phi(\xi)u-\eta(\xi)c)}{4\phi(\xi)c} & \frac{\xi}{2c} & \frac{\xi\phi'(\xi)}{4\phi(\xi)}\end{pmatrix},$$

$$\mathbf{R}=\begin{pmatrix}\mathbf{r}_1 & \mathbf{r}_2 & \mathbf{r}_3\end{pmatrix}=\begin{pmatrix}-\frac{\phi'(\xi)}{\eta(\xi)} & \frac{1}{\xi} & \frac{1}{\xi}\\ -\frac{\phi'(\xi)u}{\eta(\xi)} & \frac{u-c}{\xi} & \frac{u+c}{\xi}\\ 1 & 1 & 1\end{pmatrix},$$

where $\eta(\xi)=2\phi(\xi)-\xi\phi'(\xi)$. Then one may interpolate conservative variables via the following steps.

- First of all, the vector $\mathbf{Q}_{i+k}$ of conservative variables is projected into the characteristic space via
$$\widetilde{\mathbf{Q}}_{i+k}=\mathbf{L}_{i+\frac{1}{2}}\mathbf{Q}_{i+k},\quad k=-2,\cdots,3, \tag{2.9}$$
where the eigen-matrices $\mathbf{L}_{i+\frac{1}{2}}$ and $\mathbf{R}_{i+\frac{1}{2}}$ are linearized by algorithmic averages at each cell interface.
- Secondly, perform the WENO interpolation on the characteristic variables to obtain $\widetilde{\mathbf{Q}}^-_{i+\frac{1}{2}}=W^-_{i+\frac{1}{2}}[\widetilde{\mathbf{Q}}]$, which is done component-by-component.
- Finally, project the interpolated values $\widetilde{\mathbf{Q}}^-_{i+\frac{1}{2}}$ back into the physical space to obtain
$$\mathbf{Q}^-_{i+\frac{1}{2}}=\mathbf{R}_{i+\frac{1}{2}}\widetilde{\mathbf{Q}}^-_{i+\frac{1}{2}}. \tag{2.10}$$

Remark 2.1. To utilize the characteristic projections for the bottom topography b, we define $\mathbf{B}=(0,b,0)^T$ and follow the steps above with the same eigen-matrices $\mathbf{L}_{i+\frac{1}{2}}$ and $\mathbf{R}_{i+\frac{1}{2}}$. Then the second entry in the resulting interpolated vector $\mathbf{B}^-_{i+\frac{1}{2}}$ is denoted by $b^-_{i+\frac{1}{2}}$. The interface value approximated from right, denoted by $\mathbf{Q}^+_{i+\frac{1}{2}}$, and $\mathbf{B}^+_{i+\frac{1}{2}}$ can be done similarly. Later we will see that the first and third entries are always zero.

2.3 Spatial discretization

Based on the previous sections, a semi-discretized fifth-order AWENO scheme of the model (1.1) reads

$$\frac{\partial\mathbf{Q}}{\partial t}\Big|_{x_i}+\frac{1}{\Delta x}\left(\widehat{\mathbf{F}}_{i+\frac{1}{2}}-\widehat{\mathbf{F}}_{i-\frac{1}{2}}\right)=-gh_i\phi(\xi_i)\frac{1}{\Delta x}\left(\widehat{\mathbf{B}}_{i+\frac{1}{2}}-\widehat{\mathbf{B}}_{i-\frac{1}{2}}\right), \tag{2.11}$$

where $\mathbf{B}=(0\ b\ 0)^T$, and

$$\widehat{\mathbf{F}}_{i\pm\frac{1}{2}}=\mathbf{F}^{\mathrm{RP}}_{i\pm\frac{1}{2}}\left(\mathbf{Q}^-_{i\pm\frac{1}{2}},\mathbf{Q}^+_{i\pm\frac{1}{2}}\right)+\mathcal{D}_{i\pm\frac{1}{2}}[\mathbf{F}], \tag{2.12a}$$

$$\widehat{b}_{i\pm\frac{1}{2}}=\frac{1}{2}\left(b^-_{i\pm\frac{1}{2}}+b^+_{i\pm\frac{1}{2}}\right)+\mathcal{D}_{i\pm\frac{1}{2}}[b]. \tag{2.12b}$$

However, (2.11) is a standard AWENO discretization of (1.1), it is not well-balanced. In the next section, we are going to make some modifications so that our scheme is well-balanced.

3 High order well-balanced finite difference AWENO scheme

In this section, high order well-balanced conservative finite difference AWENO scheme is designed for the model (1.1), which requires a reformulation of the source term and a modification of the Lax-Friedrichs numerical flux.

3.1 Reformulation of the source term

Following the splitting technique [40], the source term is reformulated equivalently as

$$\mathbf{S}(\mathbf{Q},b)=\mathbf{A}\frac{\partial\mathbf{S}_b(b)}{\partial x}, \tag{3.1}$$

where the matrix $\mathbf{A}$ and vector $\mathbf{S}_b$ are

$$\mathbf{A}=\begin{pmatrix}0 & 0 & 0\\ -g(h+b)\phi(\xi) & \frac{1}{2}g\phi(\xi) & 0\\ 0 & 0 & 0\end{pmatrix},\qquad \mathbf{S}_b(b)=\begin{pmatrix}b\\ b^2\\ 0\end{pmatrix}, \tag{3.2}$$

respectively. To be consistent with the numerical fluxes $\widehat{\mathbf{F}}_{i\pm\frac{1}{2}}$, the numerical derivative of vector $\mathbf{S}_b$ is computed by the AWENO scheme:

$$\frac{\partial\mathbf{S}_b}{\partial x}\Big|_{x_i}=\frac{(\widehat{\mathbf{S}}_b)_{i+\frac{1}{2}}-(\widehat{\mathbf{S}}_b)_{i-\frac{1}{2}}}{\Delta x},\quad i=1,\cdots,N_x, \tag{3.3}$$

with

$$(\widehat{\mathbf{S}}_b)_{i+\frac{1}{2}}=\frac{1}{2}\left(\mathbf{S}_b(b^-_{i+\frac{1}{2}})+\mathbf{S}_b(b^+_{i+\frac{1}{2}})\right)+\mathcal{D}_{i+\frac{1}{2}}[\mathbf{S}_b]. \tag{3.4}$$

In general, $h^\pm_{i+\frac{1}{2}}+b^\pm_{i+\frac{1}{2}}\neq$const when the solutions to the model (1.1) are at the steady state (1.3) since the WENO operator W is nonlinear. As a result, the well-balanced property would be destroyed. To remedy this, we linearize the WENO operator as follows.

- Suppose $\widetilde{\mathbf{Q}}$ and $\widetilde{\mathbf{B}}$ have been obtained by

$$\widetilde{\mathbf{Q}}=\mathbf{L}\mathbf{Q}=(\widetilde{q}_1\,\widetilde{q}_2\,\widetilde{q}_3)^T \quad \text{and} \quad \widetilde{\mathbf{B}}=\mathbf{L}\mathbf{B}=(\widetilde{b}_1\,\widetilde{b}_2\,\widetilde{b}_3)^T.$$

- Then, the WENO operator are employed to the vector $\widetilde{\mathbf{Q}}$, i.e.,

$$W^-_{i+\frac{1}{2}}[\widetilde{\mathbf{Q}}]:=\left(W^{(1),-}_{i+\frac{1}{2}}[\widetilde{q}_1] \quad W^{(2),-}_{i+\frac{1}{2}}[\widetilde{q}_2] \quad W^{(3),-}_{i+\frac{1}{2}}[\widetilde{q}_3]\right)^T.$$

- Finally, the WENO operator is linearized in the sense that

$$W^-_{i+\frac{1}{2}}[\widetilde{\mathbf{B}}]:=\left(W^{(1),-}_{i+\frac{1}{2}}[\widetilde{b}_1] \quad W^{(2),-}_{i+\frac{1}{2}}[\widetilde{b}_2] \quad W^{(3),-}_{i+\frac{1}{2}}[\widetilde{b}_3]\right)^T.$$

3.2 Modification of the numerical fluxes

In order to achieve the well-balanced property, we modify the Lax-Friedrichs flux (2.4), according to [40], as

$$\mathbf{F}^{\mathrm{RP},(\mathrm{m})}(\mathbf{Q}^-_{i+\frac{1}{2}},\mathbf{Q}^+_{i+\frac{1}{2}})=\frac{1}{2}\left(\mathbf{F}(\mathbf{Q}^-_{i+\frac{1}{2}})+\mathbf{F}(\mathbf{Q}^+_{i+\frac{1}{2}})-\lambda(\bar{\mathbf{Q}}^+_{i+\frac{1}{2}}-\bar{\mathbf{Q}}^-_{i+\frac{1}{2}})\right), \tag{3.5}$$

where $\bar{\mathbf{Q}}=[h+b\;\; hu\;\; (h+b)\xi]^T$. Since the bottom topography b is independent of the time t, this modification is justified. One can easily check that when the solutions are at the steady state (1.3), the above modified Lax-Friedrichs numerical flux becomes

$$\mathbf{F}^{\mathrm{RP},(\mathrm{m})}(\mathbf{Q}^-_{i+\frac{1}{2}},\mathbf{Q}^+_{i+\frac{1}{2}})=\frac{1}{2}\left(\mathbf{F}(\mathbf{Q}^-_{i+\frac{1}{2}})+\mathbf{F}(\mathbf{Q}^+_{i+\frac{1}{2}})\right). \tag{3.6}$$

Finally, the numerical flux defined in (2.2) is modified as

$$\widehat{\mathbf{F}}^{(\mathrm{m})}_{i+\frac{1}{2}}=\mathbf{F}^{\mathrm{RP},(\mathrm{m})}\left(\mathbf{Q}^-_{i+\frac{1}{2}},\mathbf{Q}^+_{i+\frac{1}{2}}\right)+\mathcal{D}_{i+\frac{1}{2}}[\mathbf{F}]. \tag{3.7}$$

3.3 Well-balanced property

In summary, a semi-discretized form of well-balanced finite difference AWENO scheme can be expressed as

$$\frac{\partial\mathbf{Q}}{\partial t}\Big|_{x_i}+\frac{\widehat{\mathbf{F}}^{(\mathrm{m})}_{i+\frac{1}{2}}-\widehat{\mathbf{F}}^{(\mathrm{m})}_{i-\frac{1}{2}}}{\Delta x}=\mathbf{A}_i\frac{(\widehat{\mathbf{S}}_b)_{i+\frac{1}{2}}-(\widehat{\mathbf{S}}_b)_{i-\frac{1}{2}}}{\Delta x}, \tag{3.8}$$

where $\widehat{\mathbf{F}}^{(\mathrm{m})}_{i+\frac{1}{2}}$ is the modified Lax-Friedrichs numerical flux defined in (3.7) and $\widehat{\mathbf{S}}_{i+\frac{1}{2}}$ is computed by formula (3.4) with the linearize procedure. In the following, we are going to prove that the scheme (3.17) is well-balanced.

At the steady state, the left and right eigen-matrices $\mathbf{L}$ and $\mathbf{R}$, respectively, become

$$\mathbf{L}=\begin{pmatrix}\mathbf{l}_1\\ \mathbf{l}_2\\ \mathbf{l}_3\end{pmatrix}=\begin{pmatrix}-\dfrac{\xi\eta(\xi)}{2\phi(\xi)} & 0 & \dfrac{\eta(\xi)}{2\phi(\xi)}\\ \dfrac{\xi\eta(\xi)}{4\phi(\xi)} & \dfrac{-\xi}{2c} & \dfrac{\xi\phi'(\xi)}{4\phi(\xi)}\\ \dfrac{\xi\eta(\xi)}{4\phi(\xi)} & \dfrac{\xi}{2c} & \dfrac{\xi\phi'(\xi)}{4\phi(\xi)}\end{pmatrix},\quad \mathbf{R}=\begin{pmatrix}\mathbf{r}_1 & \mathbf{r}_2 & \mathbf{r}_3\end{pmatrix}=\begin{pmatrix}-\dfrac{\phi'(\xi)}{\eta(\xi)} & \dfrac{1}{\xi} & \dfrac{1}{\xi}\\ 0 & -\dfrac{c}{\xi} & \dfrac{c}{\xi}\\ 1 & 1 & 1\end{pmatrix}.$$

The conservative variables $\mathbf{Q}_{i+k}$ and $\mathbf{B}_{i+k}$ are projected into the characteristic fields via the left eigenvector $\mathbf{L}_{i+\frac{1}{2}}$,

$$\widetilde{\mathbf{Q}}_{i+k}=\mathbf{L}_{i+\frac{1}{2}}\mathbf{Q}_{i+k}=\begin{pmatrix}-\dfrac{\xi\eta(\xi)}{2\phi(\xi)} & 0 & \dfrac{\eta(\xi)}{2\phi(\xi)}\\ \dfrac{\xi\eta(\xi)}{4\phi(\xi)} & \dfrac{-\xi}{2c} & \dfrac{\xi\phi'(\xi)}{4\phi(\xi)}\\ \dfrac{\xi\eta(\xi)}{4\phi(\xi)} & \dfrac{\xi}{2c} & \dfrac{\xi\phi'(\xi)}{4\phi(\xi)}\end{pmatrix}\begin{pmatrix}h\\ 0\\ h\xi\end{pmatrix}_{i+k}=\begin{pmatrix}0\\ \dfrac{\xi}{2}\\ \dfrac{\xi}{2}\end{pmatrix}h_{i+k}=\begin{pmatrix}\widetilde{q}_1\\ \widetilde{q}_2\\ \widetilde{q}_3\end{pmatrix}_{i+k},\quad (3.9a)$$

$$\widetilde{\mathbf{B}}_{i+k}=\mathbf{L}_{i+\frac{1}{2}}\mathbf{B}_{i+k}=\begin{pmatrix}-\dfrac{\xi\eta(\xi)}{2\phi(\xi)} & 0 & \dfrac{\eta(\xi)}{2\phi(\xi)}\\ \dfrac{\xi\eta(\xi)}{4\phi(\xi)} & \dfrac{-\xi}{2c} & \dfrac{\xi\phi'(\xi)}{4\phi(\xi)}\\ \dfrac{\xi\eta(\xi)}{4\phi(\xi)} & \dfrac{\xi}{2c} & \dfrac{\xi\phi'(\xi)}{4\phi(\xi)}\end{pmatrix}\begin{pmatrix}0\\ b\\ 0\end{pmatrix}_{i+k}=\begin{pmatrix}0\\ \dfrac{-\xi}{2c}\\ \dfrac{\xi}{2c}\end{pmatrix}b_{i+k}=\begin{pmatrix}\widetilde{b}_1\\ \widetilde{b}_2\\ \widetilde{b}_3\end{pmatrix}_{i+k},\quad (3.9b)$$

where $k=-2,\cdots,3$. The fifth order WENO interpolation method described in Section 2.2 is employed to compute the interface values $\widetilde{\mathbf{Q}}^-_{i+\frac{1}{2}}$ and then we use the linearized WENO operator to compute $\widetilde{\mathbf{B}}^-_{i+\frac{1}{2}}$, i.e.,

$$\widetilde{\mathbf{Q}}^-_{i+\frac{1}{2}}=W^-_{i+\frac{1}{2}}[\widetilde{\mathbf{Q}}]=\begin{pmatrix}0\\ W^{(2),-}_{i+\frac{1}{2}}[\widetilde{q}_2]\\ W^{(3),-}_{i+\frac{1}{2}}[\widetilde{q}_3]\end{pmatrix},\quad \widetilde{\mathbf{B}}^-_{i+\frac{1}{2}}=W^-_{i+\frac{1}{2}}[\widetilde{\mathbf{B}}]=\begin{pmatrix}0\\ W^{(2),-}_{i+\frac{1}{2}}[\widetilde{b}_2]\\ W^{(3),-}_{i+\frac{1}{2}}[\widetilde{b}_3]\end{pmatrix}.\quad (3.10)$$

We note that $W^{(2),-}_{i+\frac{1}{2}}[\cdot]=W^{(3),-}_{i+\frac{1}{2}}[\cdot]$ since $\tilde{q}_2=\tilde{q}_3$. Therefore, they are denoted by $W^-_{i+\frac{1}{2}}[\cdot]$ consistently in the following discussion. Finally, the interpolated values $\widetilde{\mathbf{Q}}^-_{i+\frac{1}{2}}$ and $\widetilde{\mathbf{B}}^-_{i+\frac{1}{2}}$

are projected back into the physical space via the right eigenvector $\mathbf{R}_{i+\frac{1}{2}}$,

$$\mathbf{Q}^-_{i+\frac{1}{2}}=\mathbf{R}_{i+\frac{1}{2}}\widetilde{\mathbf{Q}}^-_{i+\frac{1}{2}}=\begin{pmatrix}-\dfrac{\phi'(\xi)}{\eta(\xi)} & \dfrac{1}{\xi} & \dfrac{1}{\xi}\\ 0 & \dfrac{-c}{\xi} & \dfrac{c}{\xi}\\ 1 & 1 & 1\end{pmatrix}\begin{pmatrix}0\\ W^-_{i+\frac{1}{2}}[\widetilde{q}_2]\\ W^-_{i+\frac{1}{2}}[\widetilde{q}_3]\end{pmatrix}=\begin{pmatrix}W^-_{i+\frac{1}{2}}[h]\\ 0\\ W^-_{i+\frac{1}{2}}[h\xi]\end{pmatrix}, \tag{3.11a}$$

$$\mathbf{B}^-_{i+\frac{1}{2}}=\mathbf{R}_{i+\frac{1}{2}}\widetilde{\mathbf{B}}^-_{i+\frac{1}{2}}=\begin{pmatrix}-\dfrac{\phi'(\xi)}{\eta(\xi)} & \dfrac{1}{\xi} & \dfrac{1}{\xi}\\ 0 & \dfrac{-c}{\xi} & \dfrac{c}{\xi}\\ 1 & 1 & 1\end{pmatrix}\begin{pmatrix}0\\ W^-_{i+\frac{1}{2}}[\widetilde{b}_2]\\ W^-_{i+\frac{1}{2}}[\widetilde{b}_3]\end{pmatrix}=\begin{pmatrix}0\\ W^-_{i+\frac{1}{2}}[b]\\ 0\end{pmatrix}. \tag{3.11b}$$

The right limits $\mathbf{Q}^+_{i+\frac{1}{2}}$ and $\mathbf{B}^+_{i+\frac{1}{2}}$ can be computed analogously.

Due to the consistency of the WENO interpolation operators in (3.11a) and (3.11b), we have

$$h^\pm_{i+\frac{1}{2}}=W^\pm_{i+\frac{1}{2}}[h],\quad (h\xi)^\pm_{i+\frac{1}{2}}=W^\pm_{i+\frac{1}{2}}[h\xi],\quad b^\pm_{i+\frac{1}{2}}=W^\pm_{i+\frac{1}{2}}[b], \tag{3.12}$$

and at the steady state we have

$$h^\pm_{i+\frac{1}{2}}+b^\pm_{i+\frac{1}{2}}=h+b=\text{const.} \tag{3.13}$$

Theorem 3.1. *At the steady state* (1.3)*, it can be proved that*

i) $\mathbf{F}^{RP,(m)}\left(\mathbf{Q}^-_{i+\frac{1}{2}},\mathbf{Q}^+_{i+\frac{1}{2}}\right)-\frac{1}{2}\mathbf{A}_i\left(\mathbf{S}_b(b^-_{i+\frac{1}{2}})+\mathbf{S}_b(b^+_{i+\frac{1}{2}})\right)=\begin{pmatrix}0 & \frac{1}{2}C_\phi g C^2_{surf} & 0\end{pmatrix}^T$, *where* $C_\phi:=\phi(\xi)$ *and* $C_{surf}:=h+b$,

ii) $\mathcal{D}_{i+\frac{1}{2}}[\mathbf{F}]-\mathbf{A}_i\mathcal{D}_{i+\frac{1}{2}}[\mathbf{S}_b]=\mathbf{0}$,

iii) $\widehat{\mathbf{F}}^{(m)}_{i+\frac{1}{2}}-\mathbf{A}_i(\widehat{\mathbf{S}}_b)_{i+\frac{1}{2}}=\begin{pmatrix}0 & \frac{1}{2}C_\phi g C^2_{surf} & 0\end{pmatrix}^T$.

Proof. i). According to (1.3), (3.5), (3.11a) and (3.11b), it is obviously that the first and third equations hold naturally. For the second equation, we have

$$\begin{aligned}&\frac{1}{2}g\left(h^\pm_{i+\frac{1}{2}}\right)^2\phi(\xi_i)+g(h_i+b_i)\phi(\xi_i)b^\pm_{i+\frac{1}{2}}-\frac{1}{2}g\phi(\xi_i)\left(b^\pm_{i+\frac{1}{2}}\right)^2\\ =&\phi(\xi_i)\left(\frac{1}{2}g\left(\left(h^\pm_{i+\frac{1}{2}}\right)^2-\left(b^\pm_{i+\frac{1}{2}}\right)^2\right)+g(h_i+b_i)b^\pm_{i+\frac{1}{2}}\right)\\ =&\phi(\xi_i)\left(\frac{1}{2}g\left(h^\pm_{i+\frac{1}{2}}+b^\pm_{i+\frac{1}{2}}\right)\left(h^\pm_{i+\frac{1}{2}}-b^\pm_{i+\frac{1}{2}}\right)+g(h_i+b_i)b^\pm_{i+\frac{1}{2}}\right)\\ =&\frac{1}{2}C_\phi g C^2_{\text{surf}}.\end{aligned} \tag{3.14}$$

Note that $\mathbf{A}_i$ is a constant matrix due to (1.3). It is easy to check that

$$\mathbf{F}-\mathbf{A}_i\mathbf{S}_b=\mathbf{Const}. \tag{3.15}$$

Since the operator $\mathcal{D}$ is linear, we have

$$\mathcal{D}_{i+\frac{1}{2}}[\mathbf{F}]-\mathbf{A}_i\mathcal{D}_{i+\frac{1}{2}}[\mathbf{S}_b]=\mathcal{D}_{i+\frac{1}{2}}[\mathbf{F}-\mathbf{A}_i\mathbf{S}_b]=\mathbf{0}. \tag{3.16}$$

From (3.7) and (3.4), we have

$$\begin{aligned}
&\widehat{\mathbf{F}}^{(\mathrm{m})}_{i+\frac{1}{2}}-\mathbf{A}_i(\widehat{\mathbf{S}}_b)_{i+\frac{1}{2}}\\
=&\left(\mathbf{F}^{\mathrm{RP},(\mathrm{m})}\left(\mathbf{Q}^-_{i+\frac{1}{2}},\mathbf{Q}^+_{i+\frac{1}{2}}\right)+\mathcal{D}_{i+\frac{1}{2}}[\mathbf{F}]\right)-\mathbf{A}_i\left(\frac{1}{2}\left(\mathbf{S}_b(b^-_{i+\frac{1}{2}})+\mathbf{S}_b(b^+_{i+\frac{1}{2}})\right)+\mathcal{D}_{i+\frac{1}{2}}[\mathbf{S}_b]\right)\\
=&\mathbf{F}^{\mathrm{RP},(\mathrm{m})}\left(\mathbf{Q}^-_{i+\frac{1}{2}},\mathbf{Q}^+_{i+\frac{1}{2}}\right)-\frac{1}{2}\mathbf{A}_i\left(\mathbf{S}_b(b^-_{i+\frac{1}{2}})+\mathbf{S}_b(b^+_{i+\frac{1}{2}})\right)+\left(\mathcal{D}_{i+\frac{1}{2}}[\mathbf{F}]-\mathbf{A}_i\mathcal{D}_{i+\frac{1}{2}}[\mathbf{S}_b]\right)\\
=&\left(0\ \ \frac{1}{2}C_\phi g C^2_{\mathrm{surf}}\ \ 0\right)^T.
\end{aligned}$$

We finish the proof using the conclusion of i) and ii). □

Theorem 3.2. *The modified semi-discrete scheme* (3.17) *is well-balanced.*

Proof. It is a direct corollary of Theorem 3.1. □

For the temporal discretization, the third order TVD Runge-Kutta method [33] is adopted. We note that the well-balancedness is still guaranteed when the Runge-Kutta method is employed.

3.4 Extension to two dimensions

A well-balanced finite difference AWENO spatial discretization of the two-dimensional models (1.1) reads:

$$\begin{aligned}
\frac{\partial\mathbf{Q}}{\partial t}\Big|_{(x_i,y_j)}=&-\frac{\widehat{\mathbf{F}}^{(\mathrm{m})}_{i+\frac{1}{2},j}-\widehat{\mathbf{F}}^{(\mathrm{m})}_{i-\frac{1}{2},j}}{\Delta x}-\frac{\widehat{\mathbf{G}}^{(\mathrm{m})}_{i,j+\frac{1}{2}}-\widehat{\mathbf{G}}^{(\mathrm{m})}_{i,j-\frac{1}{2}}}{\Delta y}\\
&+(\mathbf{A}_x)_{i,j}\frac{(\widehat{\mathbf{S}}_b)_{i+\frac{1}{2},j}-(\widehat{\mathbf{S}}_b)_{i-\frac{1}{2},j}}{\Delta x}+(\mathbf{A}_y)_{i,j}\frac{(\widehat{\mathbf{S}}_b)_{i,j+\frac{1}{2}}-(\widehat{\mathbf{S}}_b)_{i,j-\frac{1}{2}}}{\Delta y},
\end{aligned} \tag{3.17}$$

where $\mathbf{S}_b=[b\ b^2\ 0\ 0]^T$, the explicit forms of the vectors $\mathbf{Q}$, $\mathbf{F}(\mathbf{Q})$ and $\mathbf{G}(\mathbf{Q})$ are

$$\mathbf{Q}=\begin{pmatrix}h\\hu\\hv\\h\xi\end{pmatrix},\quad \mathbf{F}(\mathbf{Q})=\begin{pmatrix}hu\\hu^2+\frac{1}{2}g\phi(\xi)h^2\\huv\\hu\xi\end{pmatrix},\quad \mathbf{G}(\mathbf{Q})=\begin{pmatrix}hv\\huv\\hv^2+\frac{1}{2}g\phi(\xi)h^2\\hv\xi\end{pmatrix}, \tag{3.18}$$

respectively, and the matrix $\mathbf{A}_x$ and $\mathbf{A}_y$ read

$$\mathbf{A}_x=\begin{pmatrix} 0 & 0 & 0 & 0 \\ -g(h+b)\phi(\xi) & \frac{1}{2}g\phi(\xi) & 0 & 0 \\ 0 & 0 & 0 & 0 \\ 0 & 0 & 0 & 0 \end{pmatrix},\ \mathbf{A}_y=\begin{pmatrix} 0 & 0 & 0 & 0 \\ 0 & 0 & 0 & 0 \\ -g(h+b)\phi(\xi) & \frac{1}{2}g\phi(\xi) & 0 & 0 \\ 0 & 0 & 0 & 0 \end{pmatrix}, \tag{3.19}$$

respectively.

To implement, one can easily extend the one-dimensional high order well-balanced conservative finite difference AWENO scheme to the two-dimensional case on the uniform meshes in a dimension-by-dimension manner. It can be verified that the extended two-dimensional scheme achieves the fifth-order of accuracy and preserves the well-balanced property.

4 Numerical results for the Ripa model

In this section, a variety of numerical examples are used to demonstrate the robustness and effectiveness of our approach for the Ripa model. In all numerical examples, the WENO parameter ε is taken as 10^{-12}, the gravitational constant is set as $g=1$, and the CFL number is chosen as 0.45. In the following, the reference solutions are obtained by the same schemes with 2000 cells.

4.1 One-dimensional test problems

4.1.1 Well-balanced property

In the first set of tests, the well-balanced property of the proposed AWENO scheme is examined. The initial conditions are still water solutions to the Ripa model, where $h+b=10$, $u=0$ and $\theta=0.1$, with two different bottom topographies,

$$\text{smooth:} \qquad b(x)=5\exp\left(-\frac{2}{5}(x-5)^2\right), \tag{4.1a}$$

$$\text{discontinuous:} \qquad b(x)=\begin{cases} 4, & \text{if } 4\le x\le 8, \\ 0, & \text{otherwise.} \end{cases} \tag{4.1b}$$

The problem is computed in $x\in[0,10]$ up to $t=0.5$, with $N_x=200$. Exact boundary conditions are employed. To demonstrate that the well-balanced property is maintained by the proposed method to the rounding error of the machine, the problem is computed using double precision, and the L^∞-norms of errors of h, hu and $h\theta$ are shown in Table 1. It can be clearly seen that the errors are at the level of rounding errors for both the smooth and discontinuous bottom topographies, which verifies that the proposed scheme maintains the expected well-balanced property.

Table 1: L^∞-norms of errors for the steady state solutions over different bottom topographies in (4.1).

	h	hu	$h\theta$
smooth	8.88E-15	5.69E-15	8.88E-16
discontinuous	5.33E-15	5.35E-15	6.66E-16

Table 2: L^∞-norms of error and convergence orders for the test case in Section 4.1.2.

N	h		hu		$h\theta$	
	L^∞-error	Order	L^∞-error	Order	L^∞-error	Order
25	1.53E-005		2.29E-005		1.06E-005	
50	4.93E-007	4.96	8.70E-007	4.72	3.21E-007	5.05
100	1.53E-008	5.01	2.77E-008	4.97	1.22E-008	4.72
200	4.70E-010	5.02	8.58E-010	5.01	4.10E-010	4.90
400	1.44E-011	5.03	2.44E-011	5.14	1.16E-011	5.14

4.1.2 Accuracy

In this set of tests, the fifth-order of accuracy of the proposed scheme is verified. Consider a smooth bottom topography $b(x)=0.1\sin(4\pi x)-1$. The initial conditions are set as

$$\begin{cases} h(x,0)=1-b(x), \\ (hu)(x,0)=0.1, \\ \theta(x,0)=1+0.01\cos(2\pi(x-0.5)). \end{cases}$$

The problem is computed in $x\in[0,1]$ up to $t=1$, and periodic boundary conditions are employed. To observe spatial accuracy, we take the time step size Δt as $(\mathrm{CFL}\Delta x/\alpha)^{5/3}$, where $\alpha=\max_u|\lambda(u)|$ with $\lambda(u)$ the eigenvalues of the Jacobian matrix $\partial\mathbf{F}/\partial\mathbf{Q}$. The reference solution computed by the proposed scheme with $N=6400$ is treated as exact solution to problem. The L^∞-norms of errors of h, hu and $h\theta$ are shown in Table 2. It is clear seen that the expected fifth-order of accuracy is achieved.

4.1.3 Riemann problem over a flat bottom

In this example, we consider a Riemann problem over a flat bottom topography $(b(x)\equiv 0)$. The initially conditions read

$$(h,u,\theta)(x,0)=\begin{cases}(5,0,3), & x<0,\\ (1,0,5), & x\geq 0.\end{cases}$$

The numerical results at $t=0.2$ with $N_x=200$ are obtained by solving the problem in $x\in[-1,1]$ with transmissive boundary conditions. It can be observed in Fig. 2 that the numerical results are in good agreement with the reference results.

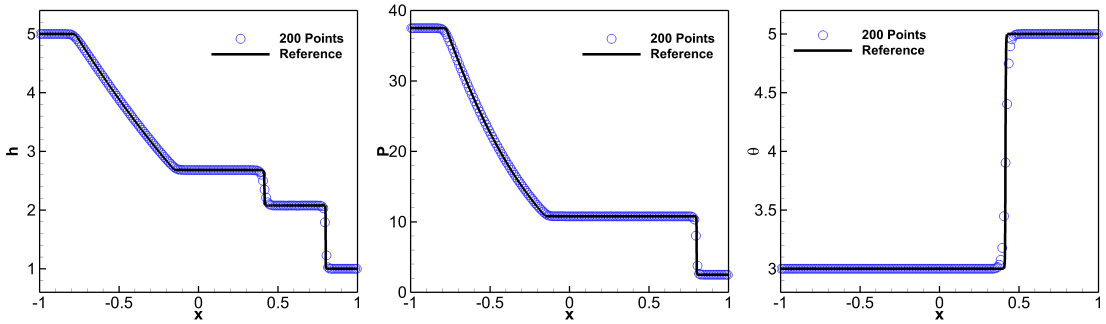

Figure 2: The numerical solutions of Riemann problem over a flat bottom in Section 4.1.3. From left to right: depth h, pressure p and temperature θ.

4.1.4 Dam break problem over a flat bottom

We consider in this set of tests the dam break problem over a flat bottom $(b(x)\equiv 0)$ with the following initial conditions

$$(h,u,\theta)(x,0)=\begin{cases}(2,0,1), & |x|\leq 0.5,\\ (1,0,1.5), & |x|>0.5.\end{cases} \tag{4.2}$$

The problem is computed in $x\in[-1,1]$ with $N_x=200$. Transmissive boundary conditions are imposed at both boundaries.

Distributions of the height h, momentum hu, temperature θ and pressure p are shown in Fig. 3 at $t=0.2$. One can observe that the physical structures are perfectly captured by our scheme.

4.1.5 Dam break problem over a rectangular bump

In this example, we extend the test problem for shallow water equations on a discontinuous water-bed presented in [37] to the Ripa model. The computational region is $[0,600]$ and the bottom topography reads

$$b(x)=\begin{cases}8, & \text{if } \ |x-300|<75,\\ 0, & \text{otherwise.}\end{cases}$$

The initial conditions for (h,u,θ) are as follows

$$(h,u,\theta)=\begin{cases}(20-b(x),0,10), & \text{if } \ x\leq 300,\\ (15-b(x),0,5), & \text{otherwise .}\end{cases}$$

The numerical results obtained at $t=12$ are shown in Fig. 4. It can be seen that the AWENO scheme captures all physical structures well, especially the steep discontinuities.

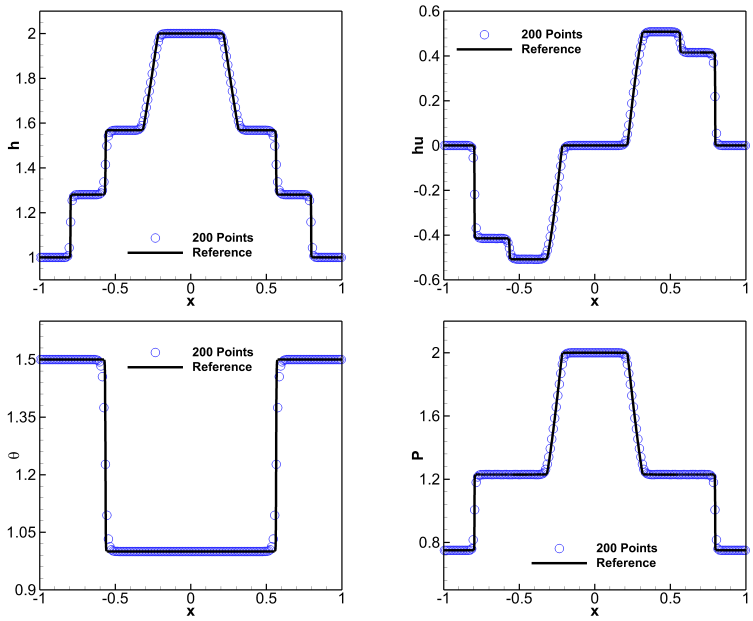

Figure 3: Distributions of the height h, momentum hu, temperature θ and pressure p of the dam break problem over a flat bottom in Section 4.1.4. Output time is $t=0.2$.

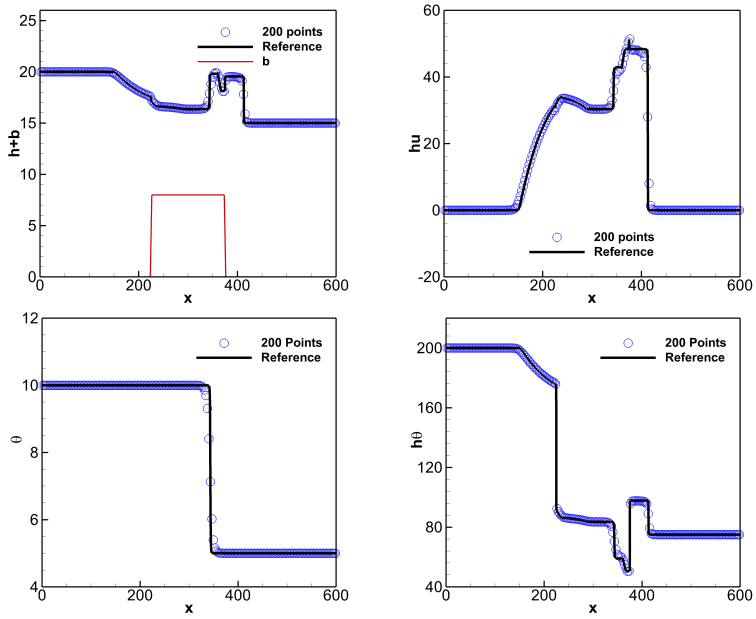

Figure 4: The numerical solutions of Riemann problem over a rectangular bump in Section 4.1.5. $h+b$ (upper left), hu (upper right), θ (lower left), and $h\theta$ (lower right).

4.2 Two-dimensional test problems

4.2.1 Well-balanced property

In this set of tests, the well-balanced property of the proposed scheme is verified by the following two-dimensional problem. The bottom consists of two Gaussian shaped humps,

$$
\begin{aligned}
b(x,y) &= \begin{cases} \frac{1}{2}\exp(-100d_l(x,y)), & x<0, \\ \frac{3}{5}\exp(-100d_r(x,y)), & x\geq 0, \end{cases} \\
d_l(x,y) &= (x+0.5)^2+(y+0.5)^2, \\
d_r(x,y) &= (x-0.5)^2+(y-0.5)^2,
\end{aligned}
$$

and the other physical quantities at the initial state read

$$
(h,u,v,\theta)(x,y,0) = \begin{cases} \left(3-b(x,y),0,0,\frac{4}{3}\right), & r<0.5, \\ (2-b(x,y),0,0,3), & r\geq 0.5, \end{cases}
$$

where $r=\sqrt{x^2+y^2}$. The problem is computed in the computational domain $(x,y)\in[-1,1]\times[-1,1]$ up to $t=0.12$. Exact boundary conditions are employed.

We compute the problem under the mesh resolution $N_x\times N_y=200\times 200$ and present 3D plots of the surface $h+b$, temperature θ and pressure p in Fig. 5. It is clear that the proposed AWENO scheme precisely maintains the steady state solutions.

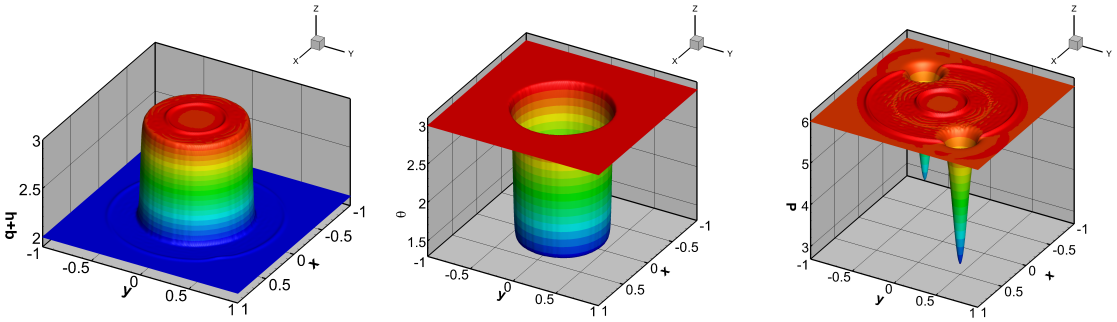

Figure 5: The 3D views of the numerical results of the steady state in Section 4.2.1. From left to right: surface, temperature and pressure.

4.2.2 Small perturbation imposed to the steady state solution

In this example, we use the same setup as in Section 4.2.1, but a small pressure perturbation is imposed to the initial depth of the water in an annular region, i.e.,

$$(h,u,v,\theta)(x,y,0)=\begin{cases}\left(3-b(x,y)+0.1,0,0,\dfrac{4}{3}\right), & 0.1\le r<0.3,\\ \left(3-b(x,y),0,0,\dfrac{4}{3}\right), & 0.3\le r<0.5, \quad \text{or} \quad r<0.1,\\ (2-b(x,y),0,0,3), & r\ge 0.5,\end{cases}$$

where $r=\sqrt{x^2+y^2}$. The problem is computed in $(x,y)\in[-1,1]\times[-1,1]$ with $N_x\times N_y=200\times 200$ up to $t=0.15$. Exact boundary conditions are used.

The 3D plots of the surface $h+b$, temperature θ and pressure p are shown in Figure 6. It can be observed that the physical structures are well resolved by our method.

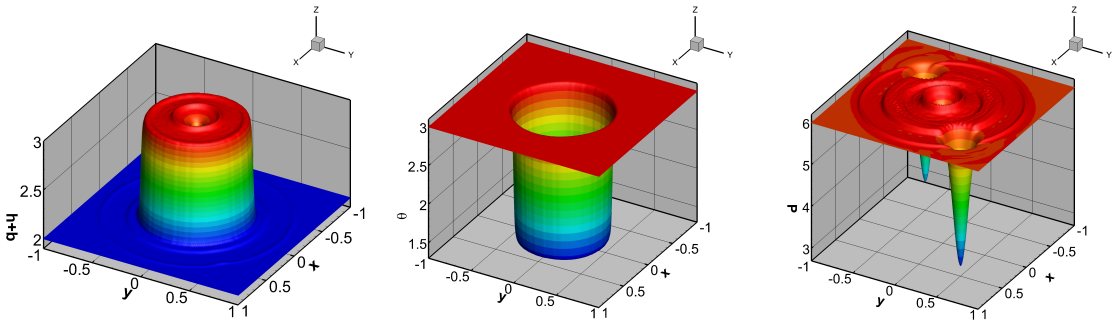

Figure 6: The 3D plots of the surface $h+b$, temperature θ and pressure p of the problem studied in Section 4.2.2. Output time is $t=0.15$.

4.2.3 Dam break problem over a flat bottom

In this example, the effectiveness of the proposed method is demonstrated by using the dam break problem. Consider a flat bottom ($b(x,y)=0$) in the computational domain $[-1,1]\times[-1,1]$ and an extremely thin dam which locates at $r=0.5$, where $r=\sqrt{x^2+y^2}$. Originally, the water depth h, velocities u and v, and temperature θ are given by

$$(h,u,v,\theta)(x,y,0)=\begin{cases}(2,0,0,1), & r<0.5,\\ (1,0,0,1.5), & r\ge 0.5.\end{cases}$$

When the dam suddenly breaks, the water inside the dam will flow outwards, due to differences in water depth and pressure. The 3D plots of the water depth h, temperature θ and pressure p are shown in Fig. 7 at $t=0.15$ with $N_x\times N_y=200\times 200$. Transmissive boundary conditions are imposed. From the figure, one can clearly observe that the fine physical structures are well captured by our scheme.

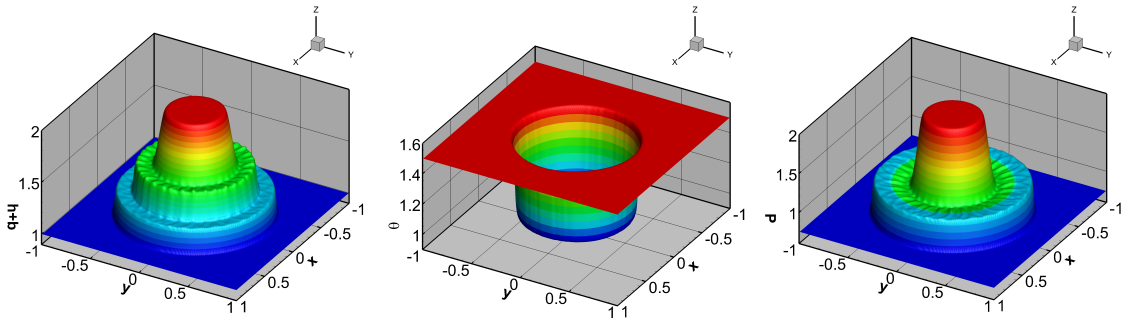

Figure 7: The 3D plots of the water depth h, temperature θ and pressure p of the dam break problem studied in Section 4.2.3. Output time is $t=0.15$.

5 Numerical results for pollutant transport model

In this section, we perform one- and two-dimensional numerical experiments of the pollutant transport models. The gravitational constant takes $g=9.812$, and other set-ups are the same as those for the Ripa model.

5.1 One-dimensional test problems

5.1.1 Well-balancedness

In this set of tests, the well-balanced property of the proposed AWENO scheme is verified. We test on two different bottom topographies, i.e., the smooth bottom

$$b(x)=5\exp\left(-\frac{2}{5}(x-5)^2\right),$$

and the discontinuous bottom

$$b(x)=\begin{cases}4, & \text{if } \ 4\leq x\leq 8,\\ 0, & \text{otherwise.}\end{cases}$$

Initially we set $h+b=10$, $u=0$ and $T=0.1$. The computational domain is $[0,10]$ with a uniform partition into 200 cells. The simulation is carried out up to $t=0.5$ with exact boundary conditions.

The L^∞-norms of errors of h, hu and hT are shown in Table 3. It can be clearly seen that the errors are at the level of rounding errors associated with double precision, which verifies that the proposed scheme is capable of maintaining the expected well-balanced property.

Table 3: L^∞-norms of errors of the surface $h+b$, velocity u and pollutant concentration T for different bottom topographies in Section 5.1.1.

	h	hu	$h\theta$
smooth	1.24E-14	1.19E-13	2.89E-15
discontinuous	1.24E-14	7.43E-14	2.44E-15

Table 4: L^∞-norms of errors and corresponding accuracies for the test problem in Section 5.1.2

.

N	h		hu		hT	
	L^∞ error	Order	L^∞ error	Order	L^∞ error	Order
25	5.65E-002		3.86E-001		5.72E-002	
50	1.51E-002	1.90	1.17E-001	1.72	1.51E-002	1.92
100	3.12E-003	2.27	2.74E-002	2.09	3.00E-003	2.33
200	2.65E-004	3.56	2.31E-003	3.57	2.56E-004	3.55
400	1.25E-005	4.41	1.06E-004	4.45	1.23E-005	4.38
800	4.13E-007	4.92	3.50E-006	4.92	4.06E-007	4.92

5.1.2 Accuracy

In this test case, the fifth-order of accuracy is verified. To observe accuracy, we take $\Delta t=(\text{CFL}\Delta x/\alpha)^{5/3}$, where $\alpha=\max_u|\lambda(u)|$ with $\lambda(u)$ being the eigenvalues of the Jacobian matrix $\partial\mathbf{F}(\mathbf{Q})/\partial Q$. The bottom topography and initial conditions are given by

$$b(x)=\sin^2(\pi x), \qquad h(x,0)=5+\exp(\cos(2\pi x)),$$
$$hu(x,0)=\sin(\cos(2\pi x)), \qquad T(x,0)=\cos(2\pi x).$$

The problem is computed in $x\in[0,1]$ up to $t=0.1$ with periodic boundary conditions, and the numerical results with $N_x=6400$ are taken as reference solutions. L^∞-norms of errors of numerical depth h, momentum hu and quantity of pollutant hT are shown in Table 4, from which the expected fifth-order of accuracy can be observed.

5.1.3 Small perturbation imposed to a steady state water body

Consider a smooth bottom topography in $x\in[0,2]$,

$$b(x)=\begin{cases}0.25(\cos(10\pi(x-1.5))+1), & 1.4\le x\le 1.6,\\ 0, & \text{otherwise},\end{cases}$$

and a small perturbation ε in water depth imposed to the steady state solutions,

$$h(x,0)=\begin{cases}1-b(x)+\varepsilon, & 1.1\le x\le 1.2,\\ 1-b(x), & \text{otherwise},\end{cases} \quad u(x,0)=0, \quad T(x,0)=0.1.$$

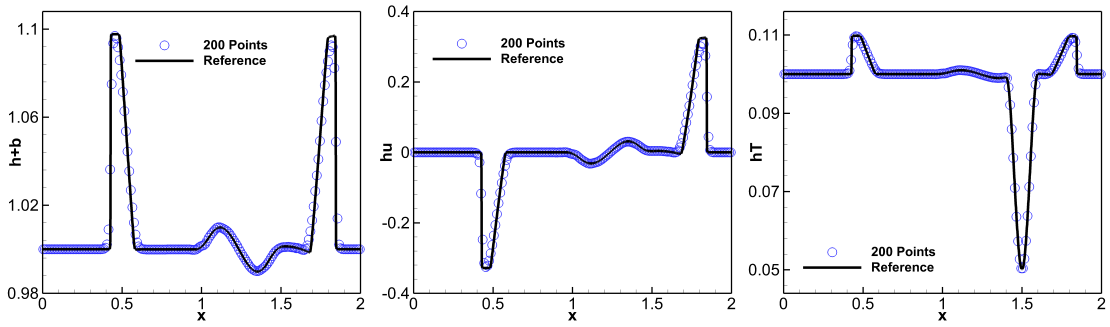

Figure 8: Numerical surface $h+b$, momentum hu and quantity of pollutant hT with $N_x=200$ for small perturbation problem in Section 5.1.3. The final time is $t=0.2$.

Later on, the flow varies rapidly due to this perturbation. The problem is simulated with $\varepsilon=0.2$ and $N_x=200$ up to $t=0.2$, with transmissive boundary conditions.

Fig. 8 shows numerical surface $h+b$, momentum hu and quantity of pollutant hT computed by our fifth-order finite-difference AWENO scheme. One may observe that the numerical solutions agree well with the reference ones, and are oscillation-free, which verifies the effectiveness of our approach.

5.1.4 Shocks over a step

We consider the pollutant transport model on a stepping bottom topography defined in $x\in[-10,10]$ as follows,

$$b(x)=\begin{cases}0, & x\leq 0,\\ 1, & x>0.\end{cases}$$

Initially, the water depth h, velocity u and pollutant concentration T are given by

$$h(x,0)=\begin{cases}4, & x\leq 0,\\ 1, & x>0,\end{cases}\qquad u(x,0)=\begin{cases}5, & x\leq 0,\\ -0.9, & x>0,\end{cases}\qquad T(x,0)=0.1.$$

The problem is computed up to $t=1$ with transmissive boundary conditions.

Fig. 9 shows numerical surface $h+b$, momentum hu and quantity of pollutant hT, which agree with those presented in [25,43]. Besides, a small perturbation in momentum can be observed at the discontinuity of bottom topography, which is not surprising since moving water steady states cannot be preserved by the current approach.

5.2 2D numerical results

5.2.1 Circular dam break

In this test example, numerical solutions [24,34] of a two-dimensional circular dam break problem are presented. At the beginning, an infinitely thin circular wall with a radius of

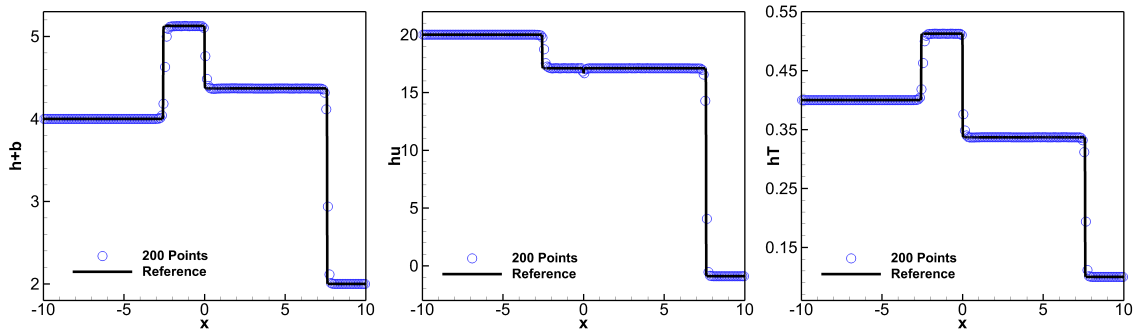

Figure 9: Numerical surface $h+b$, momentum hu and quantity of pollutant hT for problem in Section 5.1.4.

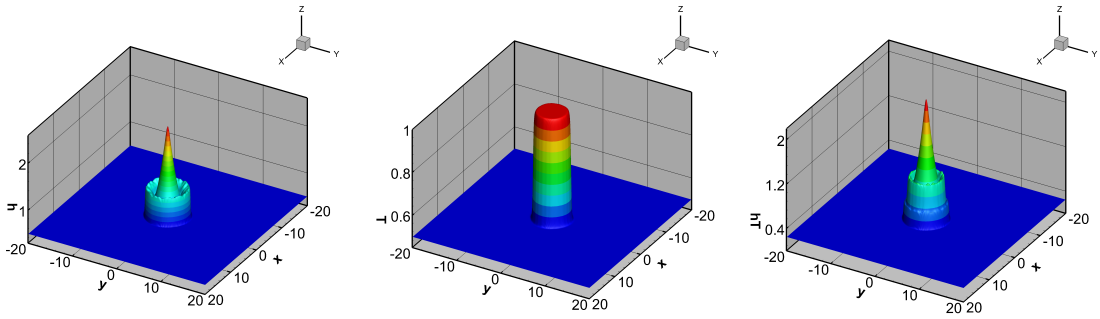

Figure 10: Numerical water depth h, concentration of pollutant T and quantity of pollutant hT for circular dam break at time $t=0.45$.

$r=\sqrt{x^2+y^2}=2.5$ is assumed in the computational domain $(x,y)\in[-20,20]\times[-20,20]$. The initial conditions are

$$(h,u,v,T)=\begin{cases}(2.5,0,0,1), & r\leq 2.5,\\ (0.5,0,0,0.5), & r>2.5.\end{cases} \tag{5.1}$$

When dam collapses instantaneously, the flow becomes transcritical due to the difference in depth outside and inside of the dam. The problem is computed with $N_x\times N_y=300\times 300$ up to $t=0.45$, and transmissive boundary conditions are set at all boundaries. Numerical results for water depth h, pollutant concentration T and hT are presented in Fig. 10. We observe that the results agree well with those in [24,34].

5.2.2 Dam break on a non-flat bottom with nonzero source

We consider the two-dimensional dam-break problem on the square domain $[-300,1100]\times[0,1400]$ with a non-flat bottom topography, the initial data is shown at the first panel of

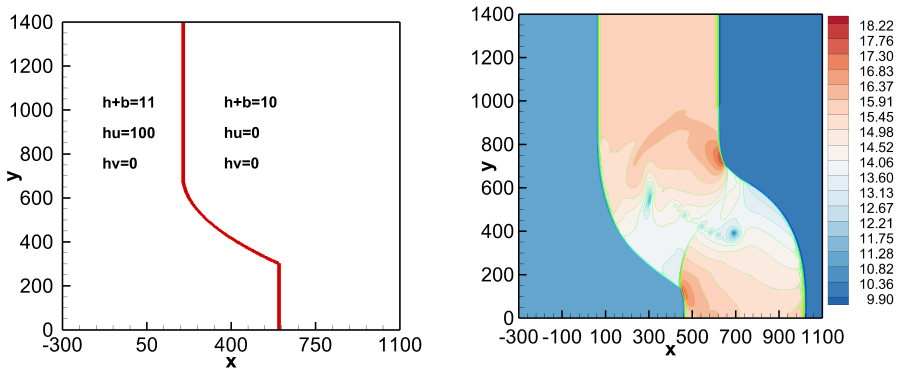

Figure 11: Initial setting in Example 5.2.2 (left) and contour plot of $h+b$ at $t=30$ (right).

Fig. 11. The shape of the dam is given by

$$\Gamma(y)=\begin{cases}\min\left[200+\dfrac{(y-700)^2}{400},600\right], & \text{if } 0\le y<700,\\ 200, & \text{if } 700\le y\le 1400.\end{cases}$$

In this example, the bottom consists of three elliptic-shaped exponential humps:

$$b(x,y)=4.5\left[\mathrm{e}^{-\kappa_1(x-500)^2-\kappa_2(y-700)^2}+\mathrm{e}^{-\kappa_2(x-300)^2-\kappa_1(y-600)^2}+\mathrm{e}^{-\kappa_2(x-700)^2-\kappa_1(y-700)^2}\right],$$

with $\kappa_1=10^{-4}$ and $\kappa_2=10^{-3}$. The water is clean at the beginning, but a source of polluted water with the concentration of pollutant $T_s=25$ is imposed immediately

$$S(x,y,t)=0.5\mathrm{e}^{-0.5(t-8)^2-0.00001(x+y-1000)^2-0.0005(x-y+200)^2}.$$

The problem is computed with $N_x\times N_y=500\times 500$ up to $t=30$. We can see from the second panel of Fig. 11 that the proposed AWENO scheme can capture fine structures generated by interactions between the initial curved shock and the complicated bottom topography.

6 Conclusions

In this paper, we propose a fifth-order finite difference AWENO scheme for the Ripa model and the pollutant transport model in a unified framework. Then by reformulating the source terms and linearizing the WENO interpolation operator, the proposed scheme is well-balanced. Finally, numerical examples verify the well-balanced property and high-order accuracy of our approach. Besides, the potential of the proposed scheme in capturing physical structures, e.g., rarefaction and shock waves, is illustrated by numerous examples.

Acknowledgements

The research of Yue Liu and Zhen Gao was partially supported by the National Key Research and Development Program of China (No. 2021YFF0704002). The research of Peng Li was supported by the Natural Science Foundation of Hebei Province, China (No. A2020210047) and National Natural Science Foundation of China (No. 11801383). The research of Yaguang Gu was supported by the National Natural Science Foundation of China (No. 12301505) and the China Postdoctoral Science Foundation (No. 2021M703040).

References

[1] F. ALCRUDO AND P. GARCIA-NAVARRO, *A high-resolution Godunov-type scheme in finite volumes for the 2D shallow-water equations*, Int. J. Numer. Methods Fluids, 16 (2010), pp. 489–505.
[2] E. AUDUSSE AND M.-O. BRISTEAU, *Transport of pollutant in shallow water: a two time steps kinetic method*, ESAIM: Math. Model. Numer. Anal., 37 (2003), pp. 389–416.
[3] D. S. BALSARA AND C.-W. SHU, *Monotonicity preserving weighted essentially non-oscillatory schemes with increasingly high order of accuracy*, J. Comput. Phys., 160 (2000), pp. 405–452.
[4] R. BORGES, M. CARMONA, B. COSTA, AND W. S. DON, *An improved weighted essentially non-oscillatory scheme for hyperbolic conservation laws*, J. Comput. Phys., 227 (2008), pp. 3191–3211.
[5] G. JIANG, AND C.-W. SHU, *Efficient implementation of weighted ENO schemes*, J. Comput. Phys., 126 (1996), pp. 202–228.
[6] S. CUI, Z. TAO, AND J. ZHU, *A new fifth-order finite volume central WENO scheme for hyperbolic conservation laws on staggered meshes*, Adv. Appl. Math. Mech., 14 (2022), pp. 1059–1086.
[7] R. LI, AND W. ZHONG, *An extension of the order-preserving mapping to the WENO-Z-type schemes*, Adv. Appl. Math. Mech., 15 (2023), pp. 202–243.
[8] Y. ZHANG, AND J. ZHU, *New finite volume mapped unequal-sized WENO scheme for hyperbolic conservation laws*, Adv. Appl. Math. Mech., 16 (2024), pp. 459–492.
[9] F. BOUCHUT, *Nonlinear stability of finite volume methods for hyperbolic conservation laws and well-balanced schemes for sources*, Frontiers in Mathematics, Birkhäuser Verlag, Basel, 2004.
[10] M.-O. BRISTEAU AND B. PERTHAME, *Transport of pollutant in shallow water using kinetic schemes*, ESAIM: Proceedings, 10 (1999), pp. 9–21.
[11] A. CANESTRELLI, A. SIVIGLIA, M. DUMBSER, AND E. F. TORO, *Well-balanced high-order centred schemes for non-conservative hyperbolic systems. applications to shallow water equations with fixed and mobile bed*, Adv. Water Res., 32 (2009), pp. 834–844.
[12] M. CASTRO, J. M. GALLARDO, AND C. PARÉS, *High order finite volume schemes based on reconstruction of states for solving hyperbolic systems with nonconservative products. Applications to shallow-water systems*, Math. Comput., 75 (2006), pp. 1103–1134.
[13] J. LI, G. LI, S. QIAN, AND J. GAO, *High-order well-balanced finite volume WENO schemes with conservative variables decomposition for shallow water equations*, Adv. Appl. Math. Mech., 13 (2021), pp. 827–849.
[14] X. LI, G. LI, AND Y. GE, *A new fifth-order finite difference WENO scheme for Dam-Break simulations*, Adv. Appl. Math. Mech., 13 (2021), pp. 58–82.
[15] A. CHERTOCK, A. KURGANOV, AND Y. LIU, *Central-upwind schemes for the system of shallow water equations with horizontal temperature gradients*, Numerische Mathematik, 127 (2014),

pp. 595–639.
[16] A. CHERTOCK, A. KURGANOV, AND G. PETROVA, *Finite-volume-particle methods for models of transport of pollutant in shallow water*, J. Sci. Comput., 27 (2006), pp. 189–199.
[17] P. J. DELLAR, *Common Hamiltonian structure of the shallow water equations with horizontal temperature gradients and magnetic fields*, Phys. Fluids, 15 (2003), pp. 292–297.
[18] V. DESVEAUX, M. ZENK, C. BERTHON, AND C. KLINGENBERG, *A well-balanced scheme to capture non-explicit steady states in the Euler equations with gravity*, Int. J. Numer. Methods Fluids, 81 (2016), pp. 104–127.
[19] Y. GU, Z. GAO, G. HU, P. LI, AND L. WANG, *High order finite difference alternative WENO scheme for multi-component flows*, J. Sci. Comput., 89 (2021), 52.
[20] Y. GU, Z. GAO, G. HU, P. LI, AND L. WANG, *A robust high order alternative WENO scheme for the five-equation model*, J. Sci. Comput., 88 (2021), 12.
[21] X. HAN AND G. LI, *Well-balanced finite difference WENO schemes for the Ripa model*, Comput. Fluids, 134-135 (2016), pp. 1–10.
[22] Y. JIANG, C.-W. SHU, AND M. ZHANG, *An alternative formulation of finite difference weighted ENO schemes with Lax-Wendroff time discretization for conservation laws*, SIAM J. Sci. Comput., 35 (2013), pp. A1137–A1160.
[23] A. KURGANOV AND D. LEVY, *Central-upwind schemes for the saint-venant system*, Mathematical Modelling and Numerical Analysis, 36 (2002), pp. 397–425.
[24] G. LI, J. GAO, AND Q. LIANG, *A well-balanced weighted essentially non-oscillatory scheme for pollutant transport in shallow water*, Int. J. Numer. Methods Fluids, 71 (2013), pp. 1566–1587.
[25] Q. LIANG AND A. BORTHWICK, *Adapive quadtree simulation of shallow flows with wet-dry fronts over complex topography*, Comput. Fluids, 38 (2009), pp. 221–234.
[26] S. F. LIOTTA AND R. G. RUSSO, *Central schemes for balance laws of relaxation type*, SIAM J. Numer. Anal., 38 (2001), pp. 1337–1356.
[27] H. LIU, *A numerical study of the performance of alternative weighted ENO methods based on various numerical fluxes for conservation law*, Appl. Math. Comput., 296 (2017), pp. 182–197.
[28] S. NOELLE, Y. XING, AND C.-W. SHU, *High-order well-balanced finite volume WENO schemes for shallow water equation with moving water*, J. Comput. Phys., 226 (2007), pp. 29–58.
[29] S. QIAN, G. LI, F. SHAO, AND Q. NIU, *Well-balanced central WENO schemes for the sediment transport model in shallow water*, Comput. Geosci., 22 (2018), pp. 763–773.
[30] J. QIU AND C.-W. SHU, *On the construction, comparison, and local characteristic decomposition for high-order central WENO schemes*, J. Comput. Phys., 183 (2002), pp. 187–209.
[31] P. RIPA, *Conservation laws for primitive equations models with inhomogeneous layers*, Geophys. Astrophys. Fluid Dyn., 70 (1993), pp. 85–111.
[32] P. RIPA, *On improving a one-layer ocean model with thermodynamics*, J. Fluid Mech., 303 (1995), pp. 169–201.
[33] C.-W. SHU AND O. STANLEY, *Efficient implementation of essentially non-oscillatory shock-capturing schemes*, J. Comput. Phys., 77 (1988), pp. 439–471.
[34] E. F. TORO, Shock-Capturing Methods for Free-Surface Shallow Flows, Wiley-Blackwell, 2001.
[35] R. TOUMA AND C. KLINGENBERG, *Well-balanced central finite volume methods for the Ripa system*, Appl. Numer. Math., 97 (2015), pp. 42–68.
[36] M. E. VÁZQUEZ-CENDÓN, *Improved treatment of source terms in upwind schemes for the shallow water equations in channels with irregular geometry*, J. Comput. Phys., 148 (1999), pp. 497–526.
[37] N. ČRNJARIĆ ŽIC, S. VUKOVIĆ, AND L. SOPTA, *Balanced central NT schemes for the shallow water equations*, in Proceedings of the Conference on Applied Mathematics and Scientific

Computing, Springer, Dordrecht, 2005, pp. 171–185.
[38] B.-S. WANG, P. LI, AND Z. GAO, *High-order well-balanced and positivity-preserving finite-difference AWENO scheme with hydrostatic reconstruction for shallow water equations*, Appl. Numer. Math., 181 (2022), pp. 483–502.
[39] B.-S. WANG, P. LI, Z. GAO, AND W. S. DON, *An improved fifth order alternative WENO-Z finite difference scheme for hyperbolic conservation laws*, J. Comput. Phys., 374 (2018), pp. 469–477.
[40] Y. XING AND C.-W. SHU, *High order finite difference WENO schemes with the exact conservation property for the shallow water equations*, J. Comput. Phys., 208 (2005), pp. 206–227.
[41] Y. XING, C.-W. SHU, AND S. NOELLE, *On the advantage of well-balanced schemes for moving-water equilibria of the shallow water equations*, J. Sci. Comput., 48 (2011), pp. 339–349.
[42] Z. XU AND C.-W. SHU, *Anti-diffusive finite difference WENO methods for shallow water with transport of pollutant*, J. Comput. Math., 24 (2006), pp. 239–251.
[43] J. ZHOU, D. CAUSON, C. MINGHAM, AND D. INGRAM, *The surface gradient method for the treatment of source terms in the shallow-water equations*, J. Comput. Phys., 168 (2001), pp. 1–25.